Feasibility of studying astrophysically important charged-particle emission with the Variable Energy γ-ray system (VEGA) at Extreme Light Infrastructure – Nuclear Physics (ELI-NP)

H.Y. Lan,[1] W. Luo,[1,*] Y. Xu,[2,†] D.L. Balabanski,[2] G.L. Guardo,[3] M. La Cognata,[3]

D. Lattuada,[3,4] C. Matei,[2] R.G. Pizzone,[3] T. Rauscher,[5,6] and J.L. Zhou[1]

[1]*School of Nuclear Science and Technology,*

University of South China, Hengyang, 421001, China

[2]*Extreme Light Infrastructure - Nuclear Physics (ELI-NP),*

Horia Hulubei National Institute for R&D in Physics and Nuclear Engineering (IFIN-HH),

30 Reactorului Str., 077125 Buchurest-Magurele, Romania

[3]*INFN-Laboratori Nazionali del Sud, 95123, Catania, Italy*

[4]*Università degli Studi di Enna KORE Viale delle Olimpiadi, 94100, Enna, Italy*

[5]*Department of Physics, University of Basel, 4056 Basel, Switzerland*

[6]*Centre for Astrophysics Research, University of Hertfordshire,*

Hatfield AL10 9AB, United Kingdom

Abstract

In the environment of a hot plasma, as achieved in stellar explosions, capture and photodisintegration reactions proceeding on excited states in the nucleus can considerably contribute to the astrophysical reaction rate. Usually, such reaction rates including the excited-state contribution are obtained from theoretical calculations as the direct experimental determination of these astrophysical rates is currently unfeasible. Future experiments could provide constraining information on the current reaction models which would improve the predictive power of the theoretical reaction rates. In the present study, experiments of photodisintegration with charged-particle emission leading to specific excited states in the residual nucleus are proposed. The expected experimental results can be used to determine the particle-transmission coefficients in the model calculations of photodisintegration and capture reactions. With such constrained transmission coefficients, the astrophysical reaction rates especially involving the excited state contributions can be better predicted and implemented in astrophysical simulations. In particular, (γ,p) and (γ,α) reactions in the mass and energy range relevant to the astrophysical p process are considered and the feasibility of measuring them with the ELISSA detector system at the future Variable Energy γ-ray (VEGA) facility at ELI-NP (Extreme Light Infrastructure - Nuclear Physics) is investigated. To this end, in a first step 17 reactions with proton emission and 17 reactions with α emission are selected and the dependence of calculated partial cross sections on the variation of nuclear property input is tested. The simulation results reveal that, for the (γ,p) reaction on twelve targets of ^{29}Si, ^{56}Fe, ^{74}Se, ^{84}Sr, ^{91}Zr, ^{96,98}Ru, ^{102}Pd, ^{106}Cd, and ^{115,117,119}Sn, and the (γ,α) reaction on five targets of ^{50}V, ^{87}Sr, ^{123,125}Te, and ^{149}Sm, the yields of the reaction channels with the transitions to the excited states in the residual nucleus, namely (γ,X_i) with $i \neq 0$, are relevant and even dominant. Therefore, these seventeen reactions are considered in the further feasibility study. For each of the seventeen photon-induced reactions, in order to attain the detectable limit of 100 counts per day for the total proton or α-particle yields, the minimum required γ-beam energies E_{low} for the measurements are estimated. It is further found that for each considered reaction, the total yields of the charged-particle X may be dominantly contributed from one, two or three (γ,X_i) channels within a specific, narrow energy range of the incident γ-beam. If the actual measurements of these photon-induced reactions are performed in this energy range, the sum of the yields of the dominant (γ,X_i) channels can be approximated by the measured yields of the charged particle X within acceptable uncertainty. This allows to experimentally obtain the yields of the (γ,X_i) channels which

dominantly contribute to the total yields of X. Using the simulated yields, these energy ranges for each of the seventeen photon-induced reactions are derived. Furthermore, the energy spectra of the (γ, X_i) channels with $0 \leq i \leq 10$ are simulated for each considered reaction, with the incident γ-beam energies in the respective energy range as derived before. Based on the energy spectra, the identification of the individual dominant (γ, X_i) channels is discussed. It becomes evident that measurements of the photon-induced reactions with charged-particle emissions considered in this work are feasible with the VEGA+ELISSA system and will provide knowledge useful for nuclear astrophysics.

----

* wen.luo@usc.edu.cn

† yi.xu@eli-np.ro

I. INTRODUCTION

It has been suggested that 32 proton-rich isotopes (p nuclides) between selenium and mercury originate from stellar explosions [1–6]. The majority of these nuclides can be produced by photodisintegration of pre-existing seed nuclei at the high temperatures achieved in supernovae [7–16]. This is called the γ process and involves the photon-induced release of neutrons, protons, and α particles from nuclei not only at stability but also several mass units off stability towards the proton-rich side of the nuclear chart. Proton capture may also contribute for the lighter p-nuclides. In any case, the required temperatures of the stellar plasma to affect the abundances of p-nuclides are in the range of $1.5 - 3.5$ GK. At such temperatures a significant fraction of all nuclei are found in thermally excited states [17–20]. Therefore, an experimental constraint of the astrophysical reaction rates for these reactions faces two challenges: dealing with unstable targets and having to determine reactions on excited nuclear states. Astrophysical simulations use theoretical reaction rates for all of these reaction rates, with few exceptions for the lighter nuclides.

It has to be realized that there is a reciprocity relation between forward and reverse reactions and that astrophysical photodisintegration rates are directly related to astrophysical capture rates (see, e.g., [20]). Accounting for reactions on excited nuclear states is a prerequisite that this reciprocity relation holds. It has been shown that significantly fewer excited states contribute in the capture direction whereas they dominate over ground-state transitions by a few orders of magnitude in photodisintegration rates [21]. Therefore a direct measurement of a photodisintegration reaction in the laboratory, with the target nucleus being in the ground state, cannot constrain the astrophysical rate unless it is possible to assume a correlation between transitions on the ground state and on excited states [22].

Nevertheless, photodisintegration experiments can help to obtain information on nuclear properties entering the reaction models used for the prediction of the astrophysical rates. Significant efforts have been undertaken to study the photon-strength function, which is not only of interest for astrophysics but also for nuclear structure studies [23]. So far, the photodisintegration measurements have been conducted using the laser-Compton scattering γ-ray source [24–27], bremsstrahlung radiation [28–35] and Coulomb dissociation [36, 37].

Additionally, it has been suggested that photodisintegration experiments can also probe particle emission to excited states in the final nucleus and thus provide information on the

transitions needed to calculate astrophysical capture rates [38–40]. This allows to better constrain the reaction models by being able to test calculations, e.g., by using different optical potentials in the computation of the relevant transitions and comparing them to the data [41]. Since fewer excited states contribute to the capture rate than the photodisintegration rate, one can place significantly stronger limits on the astrophysically relevant rates using the former rate versus the latter rate. The photodisintegration rate can then be obtained by applying the principle of detailed balance on the improved capture rate.

Despite of the previous efforts, the available experimental information concerning charged-particle emission to final excited states still is too limited to cover all the detailed nuclear transitions needed for the calculations. The Variable Energy Gamma-ray (VEGA) system, which is being constructed at the Extreme Light Infrastructure - Nuclear Physics (ELI-NP) facility, will be able to address this issue and to provide additional data to test and improve theoretical models. Quasi-monochromatic, high-intensity γ-rays up to 19.5 MeV can be delivered by VEGA, which will unlock new research opportunities on the studies of nuclear physics [42, 43], nuclear astrophysics [41, 44–46], as well as industrial and medical applications [47–50]. The silicon strip array at ELI-NP (ELISSA) is specifically constructed for charged-particle detection in photo-nucleation reactions. It is well suited to experimentally study (γ,p) and (γ,α) reactions at energies corresponding to γ-process temperatures. It is planned to specifically investigate the cross sections of the (γ,p_i) and (γ,α_i) reaction channels that proceed via the transitions from the intermediate state of the compound nucleus to different i-th final states in the residual nucleus with proton or α-particle emissions. Thus, it will not only be possible to better constrain transitions to/from excited states in astrophysical captures in general but specifically also the prediction of capture rates on unstable target nuclides can be treated in this way as long as the compound nucleus (which is the target nucleus in photodisintegration experiments) is stable.

In this paper, the feasibility of studying photon-induced reactions of astrophysical interest with VEGA and ELISSA is investigated. We focus on proton emission from seventeen targets (^{29}Si, ^{47}Ti, ^{56}Fe, ^{73}Ge, ^{74}Se, ^{84}Sr, ^{91}Zr, ^{95}Mo, ^{96,9s8}Ru, ^{102}Pd, ^{106}Cd, ^{115,117,119}Sn, ^{132}Ba, and ^{142}Nd) and α-particle emission from seventeen targets (^{50}V, ^{67}Zn, ^{87}Sr, ^{107}Ag, ^{113,115}In, ^{119}Sn, ^{123,125}Te, ^{149,154}Sm, ^{155,156,157,158,160}Gd, and ^{207}Pd). For these seventeen (γ,p) and seventeen (γ,α) reactions, the cross sections for the transitions leading to the ground state and the first ten excited states in the residual nucleus (namely (γ,p_i) and (γ,α_i) with $0 \leq i \leq 10$)

are respectively computed in Section II, in which the sensitivities of the nuclear ingredients to the calculations are illustrated as well. In Section III, based on the features of VEGA and ELISSA at ELI-NP, the results of GEANT4 simulations for the measurements of the reactions are presented, and the feasibility of measuring the individual (γ,p_i) and (γ,α_i) reaction channels is explicitly investigated. The summary is given in Section IV.

II.   THEORY AND CALCULATION

A.   Reaction model and astrophysical reaction rate

The compound nucleus contribution (CNC) is the dominant contribution to the reaction cross sections for the production of p nuclides. It is well described by the Hauser-Feshbach reaction model [51]. This model relies on the fundamental Bohr hypothesis that the reaction occurs by means of the intermediary formation of a compound nucleus that can reach a state of thermodynamic equilibrium. It is valid if the formation and decay of the compound nucleus are independent [20, 52–55]. The Hauser-Feshbach model averages over a large number of resonances in the formation of a compound nucleus and therefore can be applied if the nuclear level density (NLD) in the compound nucleus is sufficiently high at the compound formation energy, i.e., the excitation energy at which the compound nucleus is formed. This is always fullfilled for cross sections relevant to the nucleosynthesis of the p nuclides.

In the following, $\sigma^{CNC}_{A^i+\gamma\to B^j+b}(E)$ denotes the reaction cross section for the reaction $A^i+\gamma = B^j + b$ (b = proton or α-particle), i.e., photodisintegration of the i-th state in nucleus A leading to particle emission and leaving the final nucleus B in its j-th state. Each state is characterized by a spin S^i_A, a parity π^i_A and an excitation energy E^i_A for the target A and similarly for the residual nucleus B with the spin S^j_B, the parity π^j_B and the excitation energy E^j_B. In the Hauser-Feshbach model, the cross section $\sigma^{CNC}_{A^i+\gamma\to B^j+b}(E)$ from i-th state

6

in A to j-th state in B is given by (e.g. [20, 21, 52, 56, 57])

$$\sigma_{A^i+\gamma\to B^j+b}^{CNC}(E_\gamma) = \frac{\pi}{k^2} \sum_{J=mod(S_{A^i}+S_\gamma,1)}^{l_{max}+S_{A^i}+S_\gamma} \sum_{\Pi=-1}^{1}$$

$$\frac{2J+1}{(2S_{A^i}+1)(2S_\gamma+1)} \sum_{\lambda=|J-S_{A^i}|}^{J+S_{A^i}} \sum_{l_A=|\lambda-S_\gamma|}^{\lambda+S_\gamma} \sum_{J_b=|J-S_{B^j}|}^{J+S_{B^j}} \sum_{l_f=|J_b-S_b|}^{J_b+S_b}$$

$$\delta_{C_\gamma}^\pi \delta_{C_b}^\pi \frac{\langle T_{C_\gamma,l_A,\lambda}^J(E_\gamma)\rangle \langle T_{C_b,l_f,J_b}^J(E_b)\rangle}{\sum_{Clj} \delta_C^\pi \langle T_{Clj}^J(E_C)\rangle} W_{C_\gamma l_A \lambda C_b l_f J_b}^J, \tag{1}$$

where E_γ is the incident energy of γ-photon; k the wave number of the relative motion; l_{max} the maximum value of the relative orbital momentum; J and Π the total angular momentum and parity of the compound nucleus; S_{A^i} the spin of target A^i, S_γ the spin of photon, λ the multi-polarity of the photon (total angular momentum of photon), l_A the relative orbital momentum of target A^i and photon; S_{B^j} the spin of residual nucleus B^j, S_b the spin of emitted particle (proton or α particle here), J_b the total angular momentum of emitted particle, l_f the relative orbital momentum of the residual nucleus B^j and emitted particle; E_b the energy of emitted particle; C_γ the channel label of the initial system ($A^i+\gamma$) designated by $C_\gamma = (\gamma, S_\gamma, E_\gamma, E_{A^i}, S_{A^i}, \pi_{A^i})$; C_b the channel label of the final system (B^j+b) designated by $C_b = (b, S_b, E_b, E_{B^j}, S_{B^j}, \pi_{B^j})$; $\delta_{C_\gamma}^\pi = 1$ if $\pi_{A^i}\pi_\gamma(-1)^{l_A}=\Pi$ and 0 otherwise; $\delta_{C_b}^\pi = 1$ if $\pi_{B^j}\pi_b(-1)^{l_f}=\Pi$ and 0 otherwise; π_γ the parity of photon, π_b the parity of emitted particle; $\langle T \rangle$ the transmission coefficient; $\sum_{Clj} \delta_C^\pi \langle T_{Clj}^J(E_C)\rangle$ the sum of the transmission coefficients for all possible decay channels C of the compound nucleus; and W the width fluctuation correction factor for which different approximate expressions are described and discussed in Ref. [58]. In particular, the transmission coefficient for particle emission is determined by the optical model potentials between the two interacting particles, while the photon transmission coefficient depends on the photon strength function folded with the number of available final states and thus also on the level density.

When the incident energies increase approximately above the neutron separation energy, the residual nuclei formed after the first binary reaction are populated with enough excitation energy to enable further decay by particle emission. This refers to multiple emission, which can be conventionally and sufficiently described by the mechanism of multiple compound Hauser-Feshbach decay in the energy range from the neutron separation energy up to several tens of MeV. In this mechanism, after the first binary reaction the excited state j

in the residual nucleus emits secondary and further particles if energetically permitted. The population of this excited state is given by a probability distribution of the Hauser-Feshbach decay that can be completely determined by the formula of the binary reaction. In practice, the initial compound nucleus energy for the binary emission is replaced by the excitation energy of the initial nucleus for the multiple compound emission and the calculation of the emission from the excited state is the same as the calculation of the binary reaction as shown in Eq. (1).

Coming back to the simple binary case, the cross section measured in a laboratory experiment, with the target nuclei being in their ground states ($i = 0$), is given by

$$\sigma^{CNC}(E) = \sum_j \sigma^{CNC}_{A^0 + \gamma \to B^j + b}(E) \quad , \tag{2}$$

summing over all energetically accessible final states in nucleus B (including the ground state with $j = 0$). This shows that particle-transmission coefficients can be probed by photodisintegration experiments. Reactions in an astrophysical plasma at elevated temperatures, however, have to be described differently. In addition to the ground state, also excited states are populated and therefore transitions from these excited target states also have to be included, weighted by the temperature-dependent population $P_i^A(T)$ of the excited states in nucleus A. The astrophysical photodisintegration rate $\lambda_\gamma^* = n_A L_\gamma^*$ (n_A being the number density of target nuclei in the plasma) then includes a weighted sum of rates on the individual target states [17], with L_γ^* being

$$L_\gamma^*(T) = C_\gamma \sum_i P_i^A(T) \int_0^\infty \sum_j \left\{ \sigma^{CNC}_{A^i + \gamma \to B^j + b}(E_\gamma^i) \right\} E_\gamma^{i\,2} \left[e^{E_\gamma^i/(k_B T)} - 1 \right]^{-1} dE_\gamma^i \quad , \tag{3}$$

with the plasma temperature T, the photon energy E_γ^i, the Boltzmann constant k_B, and a proportionality constant C_γ. Here the photon distribution is described by the black-body Planck spectrum at the given temperature T. The population of the excited states is given by the Boltzmann factors $P_i^A(T)$. A similar equation can be found for capture reactions,

$$R^* = F(T) \sum_j P_j^B(T) \int_0^\infty \sum_i \left\{ \sigma^{CNC}_{B^j + b \to A^i + \gamma}(E^j) \right\} E^j e^{-E^j/(k_B T)} dE^j \quad , \tag{4}$$

with the population factors $P_j^B(T)$, the c.m. energy E^j of the projectiles b, the temperature-dependent factor $F(T)$, and the capture rate being $r^* = n_B n_b R^*$. Note that the reactivity R^* plays the same role for the capture rate as L_γ^* in the calculation of the photodisintegration rate but has different dimensions. Further note that the energy E_γ^i and E^j in the integration are given relative to the excitation energy of the i-th state in A and j-th state in B, respectively. This implies that the integral in each summand has a shifted energy scale relative to the other terms in the sum. This makes it hard to see that, in fact, the sum in Eq. (3) includes many more states up to a higher excitation energy than the sum in Eq. (4) when the Q value of the capture reaction is positive. It is more readily seen when mathematically transforming the sum of integrals in Eq. (4) to a single integral (the complete derivation is given in [20]),

$$R^* = F'(T)\frac{1}{G_0^B(T)} \int\limits_0^\infty \sum_j \sum_i \frac{2J_j^B + 1}{2J_0^B + 1}\frac{E - E_j^B}{E}\sigma_{Bj+b\rightarrow A^i+\gamma}^{CNC}(E - E_j^B)Ee^{-E/(k_\mathrm{B}T)}\,\mathrm{d}E \quad . \quad (5)$$

Here, the cross section is evaluated at an energy $E - E_j^B$ and cross sections at zero or negative energy (i.e., for $E - E_j^B \leq 0$) are set to zero [17]. Excitation energy and spin of excited states in nucleus B are denoted by E_j^B and J_j^B, respectively, and $G_0^B(T)$ is the nuclear partition function normalized to the ground state spin. A similar equation can be found for the photodisintegration rate. The two expressions can be directly compared by realizing that the sum over excited states i in nucleus A must contain many more terms than the sum over states j in nucleus B because the excitation energy of the compound state is $E^C = E + Q_{\mathrm{Bb}}$ when E is the c.m. energy of the projectile in a capture reaction. Thus, a larger range of thermally excited states is contributing to the photodisintegration rates. This underlines the fact that measuring $\sigma^{CNC}(E)$ as given in Eq. (2), which only includes transitions from the ground state of the target nucleus, only determines a tiny contribution to the total astrophysical photodisintegration rate. On the other hand, such a measurement can still obtain information on the particle transitions appearing in the sum over j in Eq. (5).

A reciprocity relation between forward and reverse rates can be found, [20]

$$L_\gamma^* = R^*\mathcal{F}(T)e^{-Q_{Bb}/(k_\mathrm{B}T)} \quad , \quad (6)$$

where Q_{Bb} is the reaction Q-value of the capture reaction and $\mathcal{F}(T)$ is a temperature-dependent factor. This relation allows to compute the photodisintegration rate when the capture rate is known and vice versa. Note, however, that it only applies when the contribution of thermally excited states in the respective target nuclides are taken into account. This means that this relation only applies to proper astrophysical reaction rates as computed from Eqs. (3) and (4) but not to rates obtained from simply integrating the laboratory cross section (Eq. 2), unless the contribution of excited target states is negligible and the ground-state contribution dominates. Ground-state contributions to astrophysical reaction rates are given in [19]. It is found that for nuclides in the vicinity of the p nuclides, the ground-state contributions become negligible at γ-process temperatures. The ground-state contributions are much larger for capture reactions, as explained above, but still the contribution of the excited states cannot be neglected in many cases. Therefore studying charged-particle emission by photodisintegration in the laboratory offers a way to better constrain the calculated excited state contribution in astrophysical capture rates. In this work, we aim to apply such an approach for improving the rates implemented in astrophysical simulations of the γ process by obtaining data on photon-induced particle emission from compound nuclear states.

The typical temperature of the astrophysical plasma is $1.5 - 3.5$ GK for γ-process, corresponding to the thermal energies of $kT = 170 - 260$ keV ($k = 86.173$ keV/GK is the Blotzmann constant). The peak of the Planck photon distribution is at $1.5\ kT$ [59–61], which leads to the most probable photon energy to be in the range of $260 - 390$ keV. Such energy range is mostly covered by the excitation energies of the low-lying states (*e.g.* below 500 keV) in the residual nuclei that are produced from the photodisintegration studied in this paper. The relevant contributions to the integral in Eq. (5) at γ-process temperatures stem from an energy window of about $2 - 4$ MeV for protons and $5 - 10$ MeV for α-particles [19, 62]. This means that these are the most important c.m. energies for protons and α-particles in the astrophysical plasma. Adding the reaction Q-value to these ranges yields the compound excitation energy leading to emission of charged particles in this important energy range. Studying the particle-transmission coefficients as obtained from Eq. (1) from compound states at these excitation energies provides the best information for the astrophysical application. This is not always possible experimentally due to low charged-particle yields. A measurement at a range of higher energies, nevertheless, may also be used to test
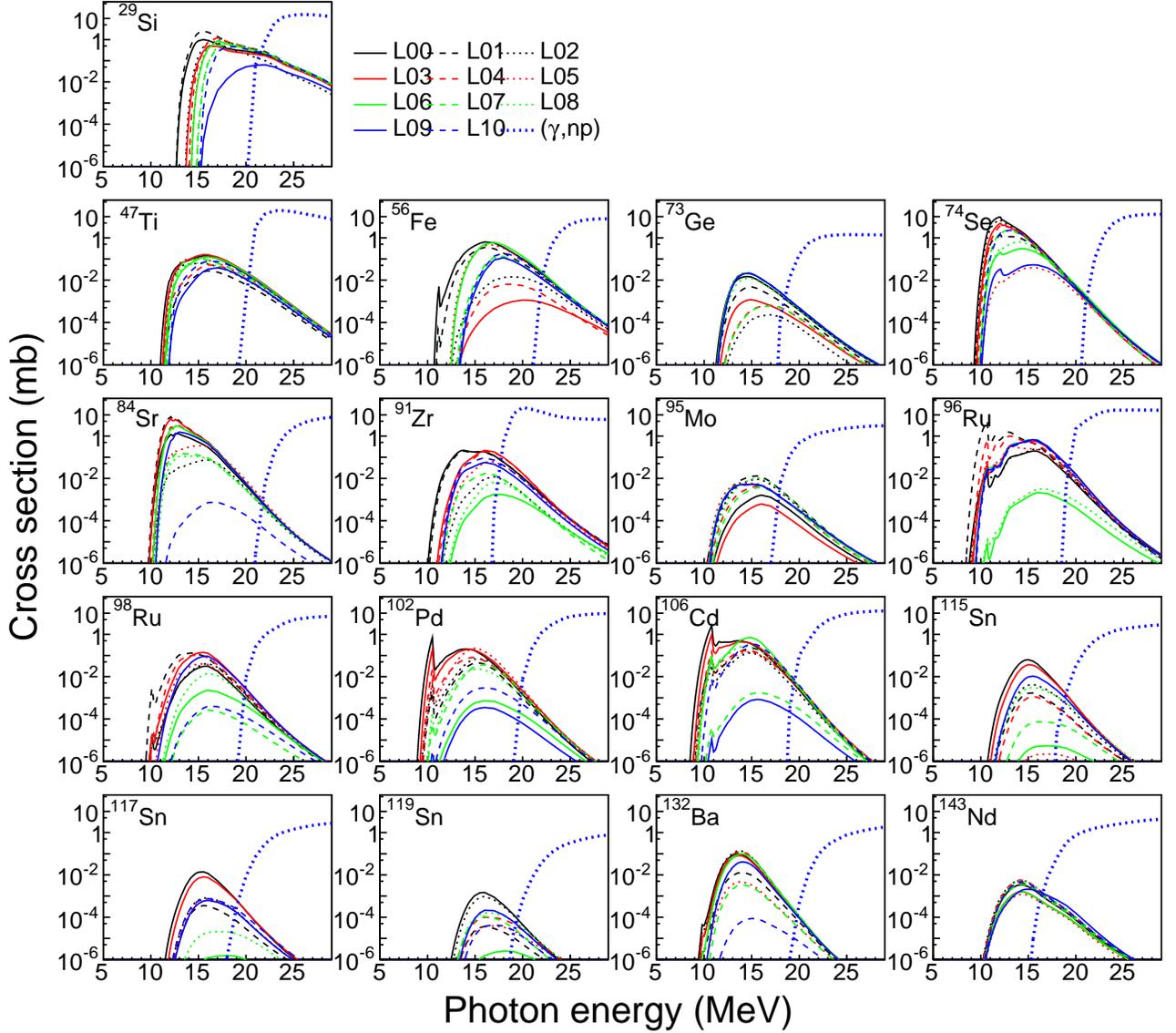
FIG. 1. The cross sections of the (γ,p_i) channels with $0 \leq i \leq 10$ and the (γ,np) channel on seventeen targets of ^{29}Si, ^{47}Ti, ^{56}Fe, ^{73}Ge, ^{74}Se, ^{84}Sr, ^{91}Zr, ^{95}Mo, ^{96,98}Ru, ^{102}Pd, ^{106}Cd, ^{115,117,119}Sn, ^{132}Ba and ^{142}Nd. The (γ,p_i) indicates the reaction with proton emission proceeding on the i-th final state ($i=0$ for the ground state) in the residual nucleus. All the results are calculated by TALYS 1.9.

the prediction of transmission coefficients and their energy dependence.

B. Photodisintegration cross sections

Among capture reactions shown to have considerable contributions of excited states to the astrophysical rate (as identified in [19]) we select cases best suited for measuring photon-
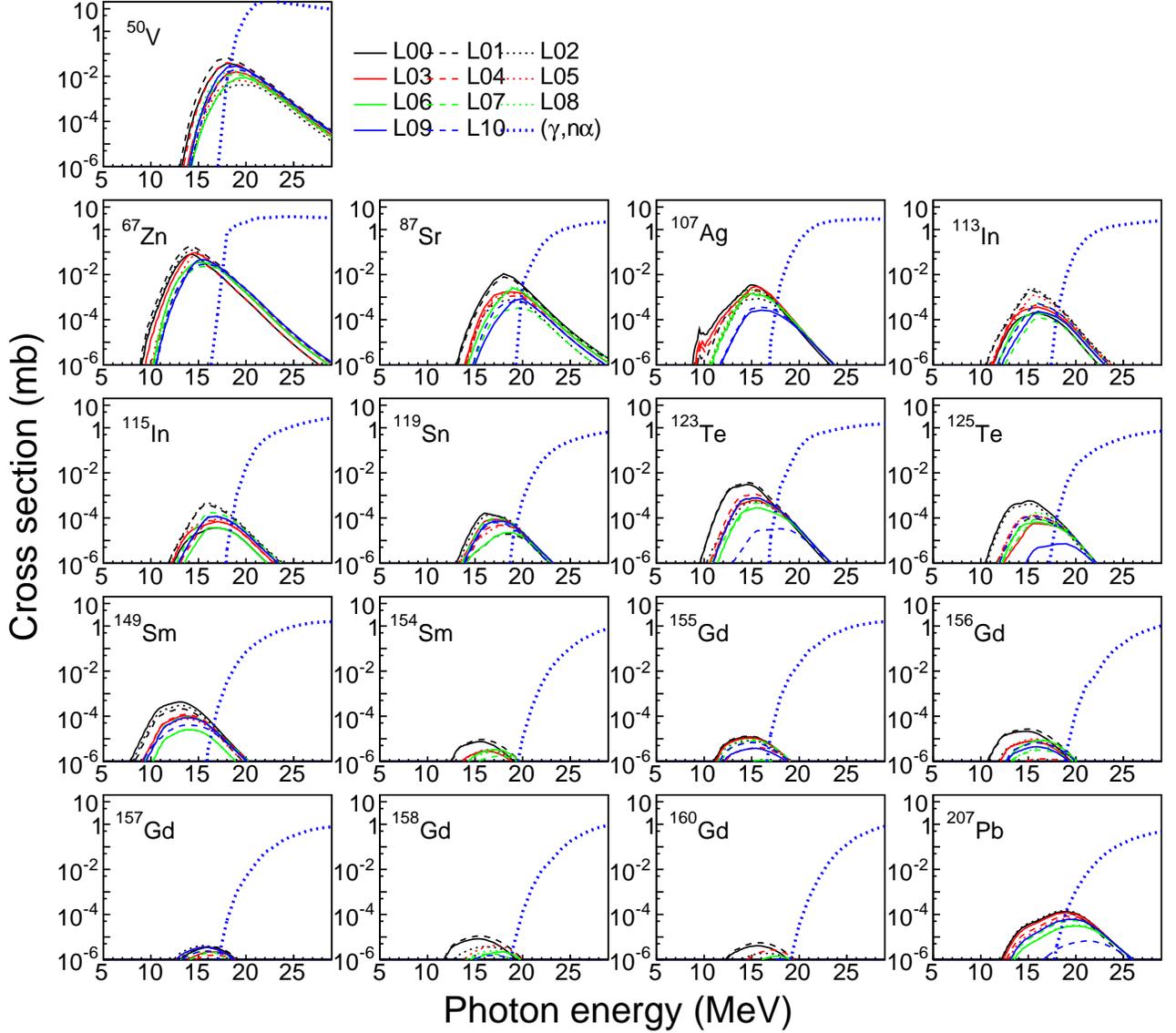
FIG. 2. The cross sections of the (γ,α_i) channels with $0 \le i \le 10$ and the $(\gamma,n\alpha)$ channel on seventeen targets of ^{50}V, ^{67}Zn, ^{87}Sr, ^{107}Ag, ^{113,115}In, ^{119}Sn, ^{123,125}Te, ^{149,154}Sm, ^{155,156,157,158,160}Gd and ^{207}Pd. The (γ,α_i) indicates the reaction with α-particle emission proceeding on the i-th final state (i=0 for the ground state) in the residual nucleus. All the results are calculated by TALYS 1.9.

induced emission to their excited states at the VEGA+ELISSA system. The photon-induced reactions with proton emission on 17 target nuclides are considered in the present study: ^{29}Si, ^{47}Ti, ^{56}Fe, ^{73}Ge, ^{74}Se, ^{84}Sr, ^{91}Zr, ^{95}Mo, ^{96,98}Ru, ^{102}Pd, ^{106}Cd, ^{115,117,119}Sn, ^{132}Ba, and ^{142}Nd. Furthermore, photon-induced α-particle emission on 17 targets are considered: ^{50}V, ^{67}Zn, ^{87}Sr, ^{107}Ag, ^{113,115}In, ^{119}Sn, ^{123,125}Te, ^{149,154}Sm, ^{155,156,157,158,160}Gd, and ^{207}Pd.

For the selected photon-induced reactions, the cross sections of (γ,p_i) and (γ,α_i) chan-

12

nels, as well as the multiple emission channels (γ,np) and $(\gamma,n\alpha)$, are computed with TALYS 1.9. The nuclear structure ingredients used in the TALYS calculations are as follows. The nuclear masses are taken from the Atomic Mass Evaluation 2016 (AME2016) [63] whenever available, while the HFB-27 nuclear masses [64] are taken into account when the AME2016 mass data are not available. The discrete experimental levels compiled in RIPL-3 library [65] and the continuum level spectrum represented by the nuclear level densities (NLDs) are both considered in the calculations. The NLDs are taken from predictions in the microscopic HFB model plus a combinatorial approach [66] that can well reproduce the low-lying cumulative number of the experimental levels. The photon strength functions obtained from the HFB plus quasiparticle random phase approximation (QRPA) [67] are used to calculate the electromagnetic transmission coefficients for the photon channel. The optical model potentials (OMPs) are employed to determine the transmission coefficient for the particle (proton and α-particle) channels. Specifically, the JLM microscopic optical potential [68] and the M3Y double folding dispersive potential [69] are used for the proton and the α-particle channels, respectively.

The calculated results for the proton emission are shown in Figure 1. The highest (γ,p_i) cross section for ^{56}Fe, ^{96}Ru and ^{102}Pd reaches about 1 mb, while that for ^{119}Sn is only a few of 10^{-3} mb. At $E_\gamma < 16$ MeV, the (γ,p_i) cross sections for the transitions to the ground state and the first two excited states ($i = 0$, 1 and 2) are dominant for most target nuclides. However, when the incident E_γ is above 16 MeV, the (γ,p_i) cross sections with $i > 2$ become relevant. This means that the transitions to the final states with higher excited energies in the residual nucleus are significant when the incident E_γ increases. Note that for the targets of ^{96}Ru and ^{98}Ru, the cross section of (γ,p_1) for the transition to the first excited state, rather than the ground state, is dominant at $E_\gamma < 16$ MeV. Furthermore, compared to the cross section of single proton emission, the cross section of multiple emission via (γ,np) is negligible for the target nuclei ^{29}Si, ^{56}Fe, ^{91}Zr and ^{96}Ru at $E_\gamma < 20$ MeV, but remarkably even dominant for ^{98}Ru, ^{102}Pd, ^{106}Cd, ^{115}Sn, ^{117}Sn and ^{119}Sn when E_γ increases above 18 MeV.

The results for the α-particle emission are shown in Figure 2. At $E_\gamma < 18$ MeV, the (γ,α_i) cross sections for the transitions to the ground and the first two excited states ($i = 0$, 1 and 2) in the residual nucleus are dominant. For the ^{50}V target, the (γ,α_1) cross section is prominent at $E_\gamma < 20$ MeV. The cross sections of $(\gamma,n\alpha)$ are comparable to those of (γ,α_i)

for ^{50}V, ^{87}Sr, ^{123}Te, and ^{149}Sm when the incident energy E_γ reaches 19 MeV.

The sensitivity of the calculated cross sections to the nuclear structure ingredients have been systematically studied in our previous work [41]. It is found that the total cross sections of (γ,p) and (γ,α) are dramatically influenced by the nuclear potentials of the charged particles. In the present study, we briefly investigate how the three kinds of nuclear structure ingredients, *i.e.*, the nuclear level density (NLD), the optical model potential (OMP), and the photon-strength function (SF), impact the contribution of the (γ,p$_i$) or (γ,α_i) cross section for a specific i-th final state in the residual nucleus to the total cross section of proton or α-particle emission. In particular, the cross section ratios of (γ,p$_1$) to (γ,p$_{tot.}$) for ^{96}Ru and (γ,α_0) to (γ,$\alpha_{tot.}$) for ^{123}Te are calculated using different sets of NLDs, OMPs and SFs available in TALYS.

The results for ^{96}Ru predicted using six sets of NLDs (1 - Constant temperature Fermi gas model [70], 2 - Back-shifted Fermi gas model [71], 3 - Generalised superfluid model [72], 4 - HFB-Skyrme model [73], 5 - HFB-Skyrme model with combinatorial method [66], and 6 - Temperature(T)-dependent HFB-Gogny model [74]), four sets of OMPs (1 - Wood-Saxon potential [75], 2 - JLMB potential with HFB-Skyrme matter density [64, 76–78], 3 - JLMB potential with HFB-Gogny matter density [76–79], and 4 - JLMB potential with HFB-Skyrme matter density plus modified imaginary part [68]), and eight sets of PSFs (1 - Generalized Lorentzian [80], 2 - Brink-Axel Lorentzian [81, 82], 3 - HFBCS-QRPA model [83], 4 - HFB-Skyrme-QRPA model [?], 5 - Hybrid model [84], 6 - T-dependent HFB-Skyrme-QRPA model [? ?], 7 - T-dependent RMF model [85], and 8 - HFB-D1M-QRPA model [86]) are shown in Figure 3(a) - 3(c). The results for ^{123}Te calculated using six sets of NLDs (same as those of ^{96}Ru), eight sets of OMPs (1 - global WS potential derived from simple folding approach [87], 2 - global WS potential for nucleus between O and U [88], 3 - double folding M3Y real plus WS volume imaginary potential [69], 4 - double folding M3Y real plus WS volume and surface imaginary potential [69], 5 - M3Y-based dispersive model potential [69], 6 - Global WS potential with surface imaginary for $40 \leq A \leq 200$ [89], 7 - Global WS potential derived from higher energy α scattering [90], and 8 - Global WS potential with the extension for lower energies [91]), and eight sets of PSFs (same as those of ^{96}Ru) are shown in Figure 3(d) - 3(f). Note that for such calculations, when a specific nuclear ingredient is changed, other nuclear ingredients generating Figure 1 and Figure 2 are kept constant. It is shown that the calculated ratios are not influenced by the changing
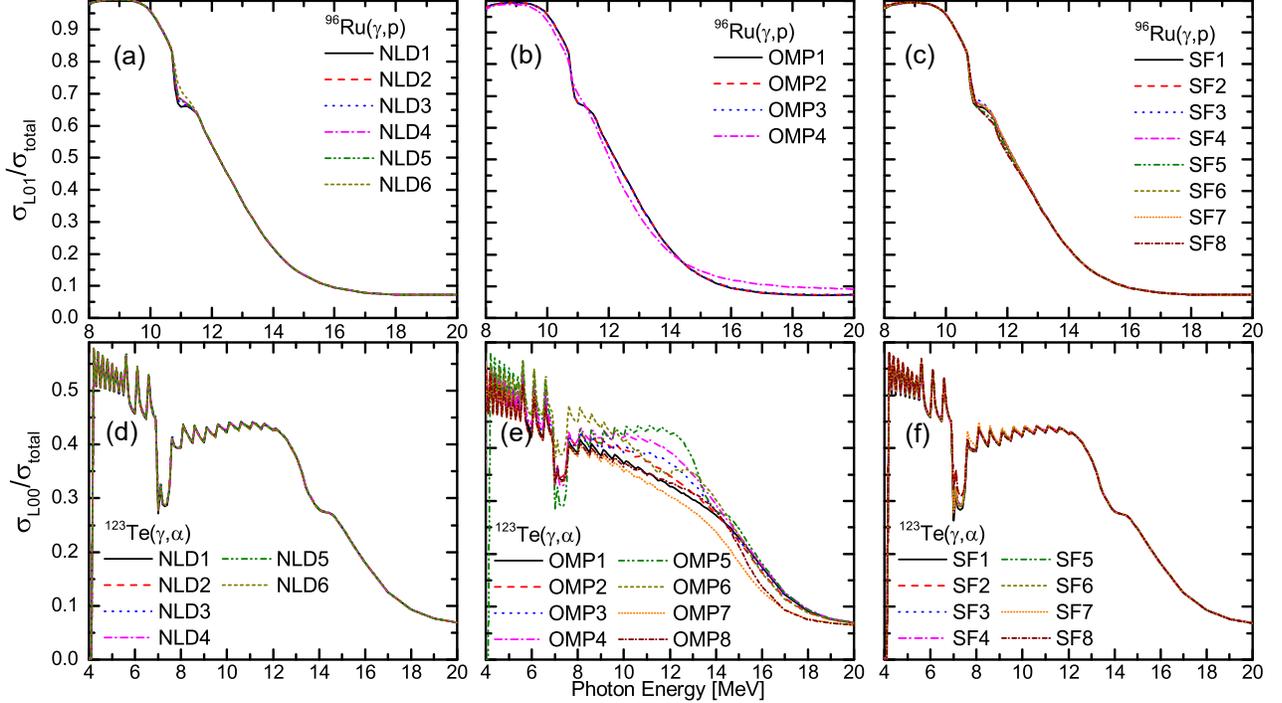
14

FIG. 3. The ratios of the (γ,p_1) cross section to the $(\gamma,p_{tot.})$ cross section for ^{96}Ru calculated with six sets of NLDs (a), four sets of OMPs (b) and eight sets of SFs (c) available in TALYS 1.9, and the ratios of the (γ,α_0) cross section to the $(\gamma,\alpha_{tot.})$ cross section for ^{123}Te calculated with six sets of NLDs (d), eight sets of OMPs (e) and eight sets of SFs (f) available in TALYS 1.9. The nuclear structure ingredients used for the calculations are indexed by numbers and described in the main text.

of NLDs and SFs, but vary within a maximum of 10% caused by different OMPs. Note that the dominance of the two studied contributions shown in Figure 3 is not impacted, regardless of the fact that different nuclear ingredients have been used in the calculation.

III. GEANT4 SIMULATION

A. Infrastructure for measurements: VEGA and ELISSA at ELI-NP

The Extreme Light Infrastructure - Nuclear Physics (ELI-NP) [42] is aiming to use extreme electromagnetic fields for nuclear physics research, which comprises a high power laser system (HPLS) and a variable energy γ-ray system (VEGA). For the VEGA at ELI-NP, the high-brilliance narrow-bandwidth γ-beam, produced via the Compton backscattering of a laser beam off a relativistic electron beam, will be delivered, with the spectral density of 5×10^3 photons/s/eV, the energies up to 19.5 MeV, and the bandwidth of 0.5%. Thanks to

such features of the γ-beam, ELI-NP could provide unique opportunities to experimentally study the photo-induced reactions of nuclear astrophysics interest.

For the detection of charged particles, at ELI-NP the silicon strip array (ELISSA) has been implemented and tested [45]. The GEANT4 simulation proves that a barrel configuration of ELISSA is particularly suited as it not only guarantees a very good resolution and granularity but also ensures a compact detection system and a limited number of electronics channels [92]. The final design of ELISSA consists of three rings of twelve X3 position sensitive detectors produced by Micron Semiconductor Ltd. [93] in a barrel-like configuration, with the assembly of four QQQ3 segmented detectors produced by Micron Semiconductor Ltd. as the end caps of both sides. Such configuration ensures a total angular coverage of $20 \leq \theta \leq 160$ in the laboratory system. The prototype of ELISSA has been constructed and tested at INFN-LNS, and the preliminary experimental results show that the energy resolution is better than 1% and that the spatial resolution is up to 1 mm [46, 94, 95].

B. Algorithm of simulation

The measurements of the photon-induced reactions on the seventeen targets with proton emission and the seventeen targets with α-particle emission are simulated using the data-based Monte Carlo simulation program GEANT4-GENBOD [96, 97]. The (γ,p_i) and (γ,α_i) channels $(0 \leq i \leq 10)$, as well as the multiple emission channels (γ,np) and $(\gamma,n\alpha)$, are taken into account in the simulation, and correspondingly the calculated cross sections in Sec. II B are incorporated as the inputs for the simulation. The features of the γ-beam facility at ELI-NP with the photon intensity of 10^4 photons/s/eV and the energy bandwidth of 1% are taken into account in the simulation, and the configuration of ELISSA is implemented. A double-layer target, consisting of a 10-μm thick target facing the γ-beam and a 0.266-μm thin carbon backing, is used in the simulation.

In order to separate the interesting charged particles produced from the photo-induced reactions, discrimination should be made on the energy spectra of the outgoing particles including electron, proton and α-particle. Our previous study [41] has suggested that the proton and the α-particle produced from the photo-induced reactions can be simultaneously measured, when the incident energy of the γ-ray (E_γ) is larger than the threshold by 1.0 - 2.0 MeV. Furthermore, it is expected that the pulse shape analysis [98] can be employed

16

to realize the particle identification of proton and α-particle. Besides the photonuclear reactions, the incident γ-beam can also induce Compton effect and pair production in the target, which may influence the detection of the energies of the emitted charged particles. In the present study, Compton effect and pair production are taken into account by invoking the electromagnetic physical process in GEANT4 simulation, and it is indicated that the rate of such background events can be removed by introducing a negligible threshold on the detector [41, 99].

C. Yield simulation and the reactions considered for further studies

For the photon-induced reactions on the seventeen targets with proton emission, the simulated yields Y_i^{p} for (γ,p_i) and Y^{np} for (γ,np) are obtained. Likewise, Y_i^α for (γ,α_i) and $Y^{\mathrm{n}\alpha}$ for $(\gamma,\mathrm{n}\alpha)$ are simulated for the seventeen photon-induced reactions with α-particle emission. The total yields $Y_{\mathrm{total}}^{\mathrm{p}}$ for the proton emission and $Y_{\mathrm{total}}^\alpha$ for the α-particle emission are respectively determined by

$$Y_{\mathrm{total}}^{\mathrm{p}} = \sum_{i=0}^{10} Y_i^{\mathrm{p}} + Y^{\mathrm{np}} \tag{7}$$

and

$$Y_{\mathrm{total}}^\alpha = \sum_{i=0}^{10} Y_i^\alpha + Y_{\mathrm{n}\alpha}. \tag{8}$$

The simulation results reveal that, for the photo-induced reactions with proton emission on twelve targets of ^{29}Si, ^{56}Fe, ^{74}Se, ^{84}Sr, ^{91}Zr, ^{96,98}Ru, ^{102}Pd, ^{106}Cd, and ^{115,117,119}Sn, and α-particle emission on five targets of ^{50}V, ^{87}Sr, ^{123,125}Te, and ^{149}Sm, the reaction yields for the transitions to the exited states in the residual nucleus are relevant and even dominant. These seventeen photo-induced reactions with the proton emission on twelve targets and the α-particle emission on five targets are further considered in the following simulation studies, because the emphasis of the present paper is to investigate the feasibility of the measurements for the photo-induced reactions proceeding on the excited states in the residual nucleus. Meanwhile, for the remaining seventeen reactions, the simulation results indicate that the reaction yield for the transition to the ground state is prominent all along the incident energies of the γ-beam, so these seventeen photo-induced reactions are no longer taken into
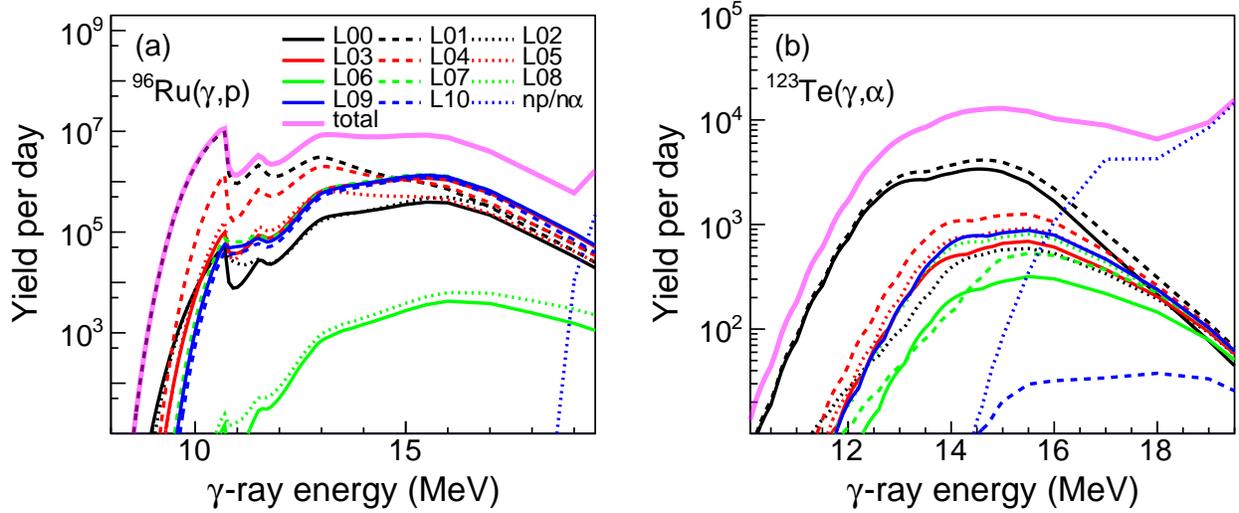
FIG. 4. (a) The simulated yields Y_i^p for ^{96}Ru(γ,p_i) with $0 \leq i \leq 10$, Y^{np} for ^{96}Ru(γ,np), and Y_{total}^p for ^{96}Ru$(\gamma,p_{tot.})$. (b) The simulated yields Y_i^α for ^{123}Te(γ,α_i) with $0 \leq i \leq 10$, $Y^{n\alpha}$ for ^{123}Te$(\gamma,n\alpha)$, and Y_{total}^α for ^{123}Te$(\gamma,\alpha_{tot.})$.

account in the present study.

As an example, figure 4 demonstrates the simulated yields Y_i^p, Y^{np} and Y_{total}^p for $\gamma + ^{96}$Ru reaction, and Y_i^α, $Y^{n\alpha}$ and Y_{total}^α for $\gamma + ^{123}$Te reaction. For ^{96}Ru, it is found that the (γ,p_1) yield is dominant up to $E_\gamma = 14$ MeV, while the (γ,p_4) channel becomes significant with the increase of the incident γ-beam energy. For ^{123}Te, the yields of the reactions proceeding on the ground state (γ,α_0) and the first excited state (γ,α_1) in the residual nucleus are comparable, which are both considerable at the entire energy range of the incident γ-beam.

D. Feasibility study for the measurement of the (γ,p_i) and (γ,α_i) channels

In order to evaluate the feasibility of the measurements for the considered seventeen photo-induced reactions, it is necessary to estimate the required energies of the incident γ-beam that can satisfy a minimum measurable limit of the experimental yield. Our previous study [41] has shown that for the measurement of the charged-particles yield, a minimum measurable limit of 100 counts per day is appropriate, considering the details of the ELISSA detector worked out in Ref. [46, 94]. For each of the seventeen photo-induced reactions considered in the present simulation studies, the total yield of proton or α-particle stemming from all the open (γ,p_i) or (γ,α_i) channels can be measured. Therefore, the minimum measurable limit of 100 counts per day for Y_{total}^p or Y_{total}^α is taken into account. To meet such

criteria, the required energies of the incident γ-beam, namely $E_{\text{req.}}$, are deduced for each of the seventeen photo-induced reactions, and the results are listed in Table I (column 4).

Furthermore, for the seventeen photo-induced reactions considered in the simulation studies, the relative contributions of the reaction yields for the transitions to different final states in the residual nucleus are investigated. In particular, the yield ratios $Y_i^{\text{p}}/Y_{\text{total}}^{\text{p}}$ and $Y_i^{\alpha}/Y_{\text{total}}^{\alpha}$ for each i-th state are calculated from the simulated yields, and the results are shown in Figure 5. Note that the minimum required energies of the γ-beam, $E_{\text{req.}}$, obtained in Sec. III C (column 4 in Table I), are set as the lower limit of the X-axis for each reaction.

In Figure 5 it can be seen that for all the reactions, when the energy of the incident γ-beam (E_γ) is lower, the contributions to the total yields from the transitions to several (usually no more than three) final states in the residual nucleus are dominant, while no prominent channels contributing to the total yields can be found when E_γ is getting higher. Therefore, for each reaction in Figure 5, if the expected experiments are performed within the specified (narrow) energy ranges of the incident γ-beam, i.e. $[E_{\text{low}}, E_{\text{upper}}]$, the total reaction yields $Y_{\text{total}}^{\text{p}}$ or $Y_{\text{total}}^{\alpha}$ will be dominantly contributed from the sum of the yields of n individual (γ,p_i) or (γ,α_i) channels, namely $\Sigma_{i \in n} Y_i^{\text{p}}$ or $\Sigma_{i \in n} Y_i^{\alpha}$, with an acceptable relative uncertainty Δ. This can be represented by:

$$(Y_{\text{total}}^{\text{p}} - \sum_{i \in n} Y_i^{\text{p}})/Y_{\text{total}}^{\text{p}} \leq \Delta \tag{9}$$

or

$$(Y_{\text{total}}^{\alpha} - \sum_{i \in n} Y_i^{\alpha})/Y_{\text{total}}^{\alpha} \leq \Delta. \tag{10}$$

In practice, the total yields $Y_{\text{total}}^{\text{p}}$ and $Y_{\text{total}}^{\alpha}$, respectively, are straightforwardly the experimental yields of proton or α-particle that can be obtained from the realistic photon-induced measurements. Therefore, $\Sigma_{i \in n} Y_i^{\text{p}}$ or $\Sigma_{i \in n} Y_i^{\alpha}$ can be derived from Eqs. 9 and 10 with the given relative uncertainty Δ. This allows us to experimentally determine the yields of the n (γ,p_i) or (γ,α_i) channels that prominently contribute to the total yields with an acceptable uncertainty. Note that such a procedure is valid only if the energies of the incident γ-beam for the photo-induced measurements are in the range of $[E_{\text{low}}, E_{\text{upper}}]$. Thus it is significant to obtain the energy range $[E_{\text{low}}, E_{\text{upper}}]$ for each of the seventeen photon-induced reactions.

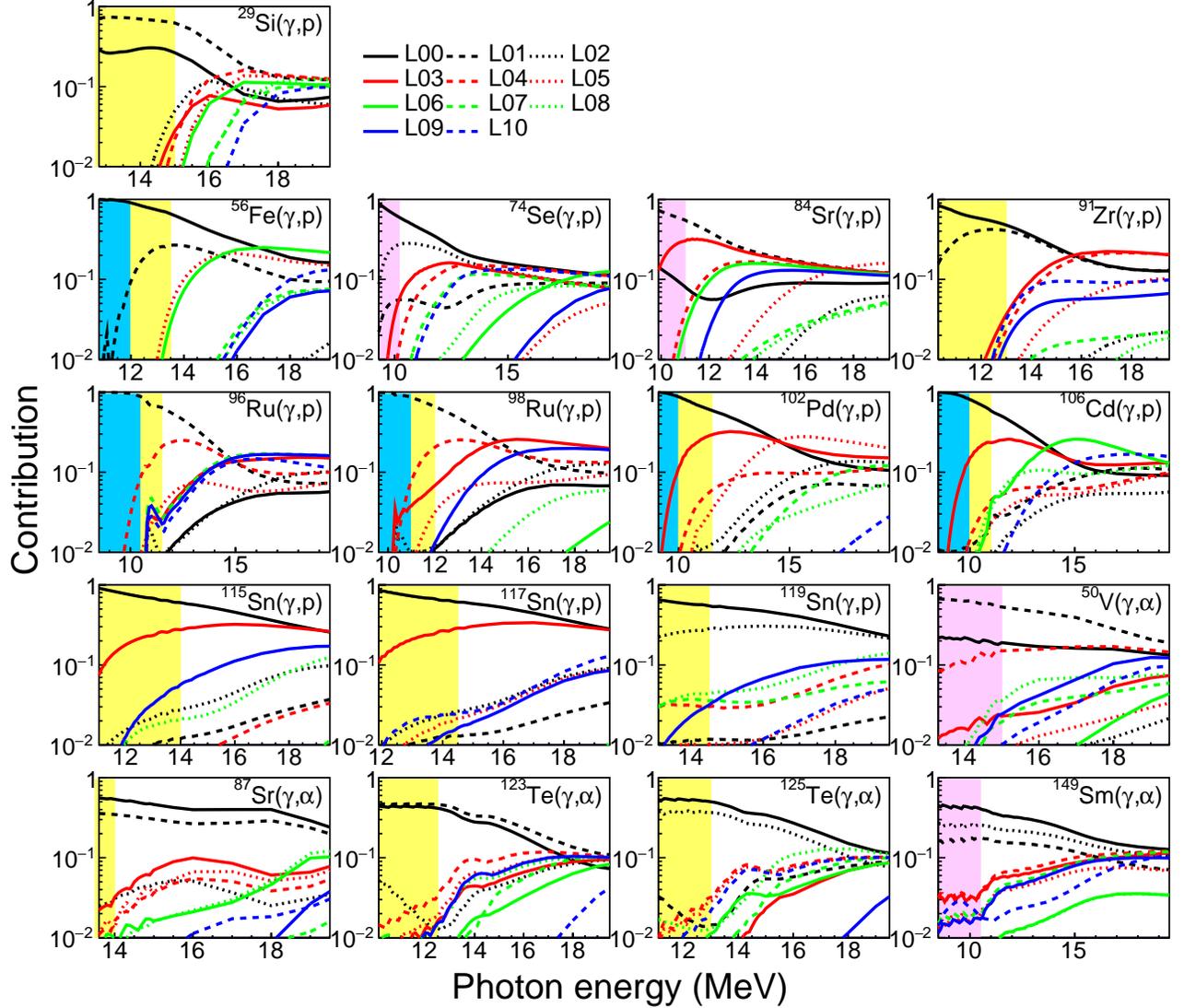As far as the present simulation is concerned, the energy range $[E_{\text{low}}, E_{\text{upper}}]$ can be

19

FIG. 5. The relative contributions of the (γ, X_i) channels (X=p or α) for each i-th final state ($0 \leq i \leq 10$) in the residual nucleus to the total yields of the charged particle X, Y_i^X/Y_{total}^X, for the considered seventeen photo-induced reactions. The blue, yellow and purple bands illustrate the energy ranges of the incident γ-beam for performing the measurements, in which one, the sum of two, and the sum of three (γ, X_i) channels respectively contribute more than 90% to the total yield of X. See the text for more details.

estimated by satisfying Eqs. 9 and 10 with the simulated yields (Y_i^X and Y_{total}^X, X=p or α) and the given n and Δ. In the present study, $[E_{\text{low}}, E_{\text{upper}}]$ corresponding to $n = 1$, 2 and 3 are respectively estimated with $\Delta = 10\%$. This means that, for $n = 1$, a single (γ, X_i) channel contributes more than 90% to the total yield Y_{total}^X, while for $n = 2$ or 3, more than 90% of the total yield is contributed from the sum of the yields of 2 or 3 (γ, X_i) channels, respectively. For each of the seventeen photon-induced reactions, the obtained

$[E_{\text{low}},E_{\text{upper}}]$ are listed in table I, and concomitantly, the identified (γ,X_i) channels that dominantly contribute to the total yields in $[E_{\text{low}},E_{\text{upper}}]$ are given as well. Meanwhile, the energy ranges $[E_{\text{low}},E_{\text{upper}}]$ for $n = 1$, 2 and 3 are respectively illustrated with the areas in blue, yellow and purple in Figure 5 for each reaction.

It can be seen in Figure 5 that, for the photo-induced reactions with proton emissions on the targets of ^{56}Fe, ^{96}Ru, ^{98}Ru, ^{102}Pd and ^{106}Cd, the single (γ,p_0) or (γ,p_1) channel prominently contributes to the total proton yield. Thus the yields of these five specific channels, ^{56}Fe(γ,p_0), ^{96}Ru(γ,p_1), ^{98}Ru(γ,p_1), ^{102}Pd(γ,p_0) and ^{106}Cd(γ,p_0), can be exclusively determined from the measurements if the energies of the incident γ-ray are in the ranges indicated by the blue areas in Figure 5. Note that if the photonuclear measurements can be performed with the incident γ-ray in the energy range illustrated by the yellow areas in Figure 5, more than 90% of the total yields stem from two specific (γ,X_i) (X=p or α) channels. Furthermore, for ^{50}V, ^{74}Se, ^{84}Sr and ^{149}Sm, the sum of the yields of three (γ,X_i) channels contribute at least 90% of the total yields, when the incident γ-ray energies are in the range shown by the purple areas in Figure 5. In this way, the sum of the yields of such two or three specific channels can be directly determined from the measured yields. However, in order to further derive the yields of each individual channel proceeding on different final excited states in the residual nucleus, the energy spectra of the emitted charged-particles are expected to be investigated for the seventeen photo-induced reactions.

E.   Energy spectra

The peak energy of the emitted particle from the photon-induced reaction $A(\gamma,X_i)B$ is calculated by

$$E_X = \frac{M_B}{M_B + M_X}(E_\gamma + Q - E_i^*), \tag{11}$$

in which M_B and M_X are the atomic mass of the residual nucleus and the emitted particle, respectively. In the present case X denotes proton or α particle; E_γ is the energy of the incident γ-beam; Q is the Q-value of the reaction $A(\gamma,X)B$; and E_i^* is the excitation energy of the i-th state in the residual nucleus B. For the photon-induced reaction $A+\gamma$ with the emissions of α and proton, the energy gap ΔE between the peaks of the emitted α and the

21

TABLE I. S_p: the proton separation energies. S_α: the α-particle separation energies. E_{req}: the required energies of the incident γ-beam for performing the measurements of which the minimum $(\gamma, p_{tot.})$ or $(\gamma, \alpha_{tot.})$ yield of 100 counts per day can be attained. $[E_{low}, E_{upper}]$: the energy range of the incident γ-beam for performing the measurements, in which the sum of the yields of 1, 2, and 3 (γ, X_i) (X=p or α) channels are respectively dominant and can be experimentally determined. Correspondingly, these dominant (γ, X_i) channels are explicitly given as well. The unit of all the energies is MeV. See the text for more details.

Reaction	S_p or S_α	E_{req}	E_{range} for $n = 1$ states	E_{range} for $n = 2$ states	E_{range} for $n = 3$ states
^{29}Si$(\gamma,p)^{28}$Al	12.30	12.70		$12.7 - 15.0$ p_0, p_1	
^{50}V$(\gamma,\alpha)^{46}$Sc	9.88	13.3			$13.3 - 15$ α_0, α_1, α_4
^{56}Fe$(\gamma,p)^{55}$Mn	10.20	10.80	10.8-12 p_0	$12 - 13.5$ p_0, p_1	
^{74}Se$(\gamma,p)^{73}$As	8.55	9.3			$9.3 - 10.2$ p_0, p_1, p_2
^{84}Sr$(\gamma,p)^{83}$Rb	8.87	9.9			$9.9 - 11.0$ p_0, p_1, p_3
^{87}Sr$(\gamma,\alpha)^{83}$Kr	7.31	13.5		$13.5 - 14.0$ α_0, α_1	
^{91}Zr$(\gamma,p)^{90}$Y	8.69	10.3		$10.3 - 13$ p_0, p_1	
^{96}Ru$(\gamma,p)^{95}$Tc	7.35	8.5	$8.5 - 10.5$ p_1	$10.5 - 11.5$ p_1, p_4	
^{98}Ru$(\gamma,p)^{97}$Tc	8.29	9.6	$9.6 - 11$ p_1	$11 - 12$ p_1, p_4	
^{102}Pd$(\gamma,p)^{101}$Rh	7.81	9.1	$9.1 - 10.0$ p_0	$10.0 - 11.5$ p_0, p_3	
^{106}Cd$(\gamma,p)^{105}$Ag	7.35	8.5	$8.5 - 10$ p_0	$10 - 11$ p_0, p_3	
^{115}Sn$(\gamma,p)^{114}$In	8.75	11		$11 - 14$ p_0, p_3	
^{117}Sn$(\gamma,p)^{116}$In	9.44	11.9		$11.9 - 14.5$ p_0, p_3	
^{119}Sn$(\gamma,p)^{118}$In	10.10	13.1		$13.1 - 14.5$ p_0, p_2	
^{123}Te$(\gamma,\alpha)^{119}$Sn	1.53	10.5		$10.5 - 12.5$ α_0, α_1	
^{125}Te$(\gamma,\alpha)^{121}$Sn	2.25	11.1		$11.1 - 13$ α_0, α_2	
^{149}Sm$(\gamma,\alpha)^{145}$Nd	0.00	8.5			8.5-10.5 α_0, α_1, α_2

emitted proton can be expressed as

$$\begin{aligned}
\Delta E &= E_\alpha - E_p \\
&= \frac{M_{(A-\alpha)}}{M_{(A-\alpha)} + M_\alpha}(E_\gamma + Q_{(\gamma,\alpha)} - E^*_{i\ (A-\alpha)}) \\
&\quad - \frac{M_{(A-p)}}{M_{(A-p)} + M_p}(E_\gamma + Q_{(\gamma,p)} - E^*_{i\ (A-p)}).
\end{aligned} \tag{12}$$

The existence of the energy gap ΔE is beneficial to the disentanglement of the emitted proton and α-particle from a photon-induced reaction, and the larger ΔE indicates the better particle identification. In Eq. 11, the excitation energy E^* of the low-lying state is usually much less than the Q-value, so the energy gap ΔE between the α-particle peak and the proton peak is determined by the discrepancy between $Q_{(\gamma,p)}$ and $Q_{(\gamma,\alpha)}$. In this case, it is demonstrated by our previous study [41] that, for most photon-induced reactions on the p-nuclei, the emitted proton and α-particle can be effectively disentangled from the energy spectra.

Furthermore, according to Eq. 11, the energy gap ΔE between the peaks of two identical charged-particles X (X = proton or α-particle), which are respectively emitted from the (γ,X_i) channels with two different i-th final states in the residual nucleus, is the difference of the excitation energies of these two final states. In the present study, for the seventeen photo-induced reactions listed in Table I, the energy spectra of (γ,X_i) are simulated with the energies of the incident γ-beam in $[E_{\text{low}},E_{\text{upper}}]$. This allows us to investigate the possibility of disentangling the identical charged-particles and obtaining the yields of the individual (γ,X_i) channels. Note that the minimum measurable limit of 100 counts per day is still taken into account for the total yields obtained from integrating the energy spectrum of each (γ,X_i).

For ^{96}Ru and ^{98}Ru, the energy spectra of the protons emitted from (γ,p_1) and $(\gamma,\text{p}_{\text{tot.}})$ channels at $E_\gamma = 10.0$ MeV are shown in Figure 6. Here $(\gamma,\text{p}_{\text{tot.}})$ denotes the proton emission proceeding on all the eleven final states in the residual nucleus. The results indicate that the protons generated by ^{96,98}Ru(γ,p_1) are dominant at $E_\gamma \simeq 10.0$ MeV ($\approx Q_{(\gamma,p)} + 2.5$ MeV). The first excited states in the residual nuclei ^{95,97}Tc are metastable (isomer) states with the half-lives of 61 and 91 days respectively, which lead to the relative larger yields and cross sections for (γ,p_1) reactions. Thus the measurements of ^{96,98}Ru(γ,p_1) at $E_\gamma = 10.0$ MeV are feasible.
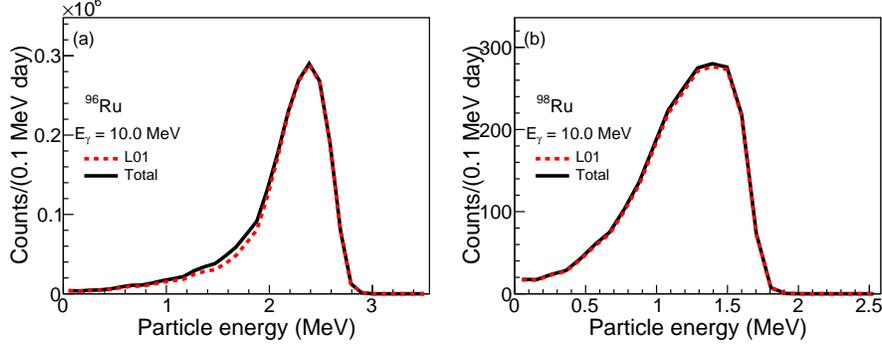
FIG. 6. Energy spectra of the protons emitted from (γ,p_1) and $(\gamma,p_{tot.})$ channels, indexed by "L01" and "Total" respectively, on ^{96}Ru target (a) and ^{98}Ru target (b) at $E_\gamma = 10.0$ MeV. The results of $(\gamma,p_{tot.})$ include the contributions from all the (γ,p_i) channels with $0 \leq i \leq 10$.

Figure 7 demonstrates the proton spectra of (γ,p_0), (γ,p_1) and $(\gamma,p_{tot.})$ on ^{29}Si target at $E_\gamma = 14.5$ MeV (a) and ^{91}Zr target at $E_\gamma = 12.0$ MeV (b), and the α-particle spectra of (γ,α_0), (γ,α_1) and $(\gamma,\alpha_{tot.})$ on ^{87}Sr target at $E_\gamma = 13.5$ MeV (c) and ^{123}Te target at $E_\gamma = 11.5$ MeV (d). From these four reactions, the reaction channels leading to the ground state and the first excited state in the residual nucleus contribute more than 90% to the total spectra of the emitted charged-particles. It can be also found that the sum of the yields of (γ,X_0) and (γ,X_1) is measurable, while the yields of the two respective channels cannot be experimentally determined.

In Figure 8 the proton spectra of (γ,p_0), (γ,p_2) and $(\gamma,p_{tot.})$ on ^{119}Sn at $E_\gamma = 14.5$ MeV (a) and the α-particle spectra of (γ,α_0), (γ,α_{12}) and $(\gamma,\alpha_{tot.})$ on ^{125}Te at $E_\gamma = 12.5$ MeV (b) are given. It is shown that the sum of the yields of (γ,X_0) and (γ,X_2) can be measured because of their dominant contributions to the total yields of all the eleven transitions. However, the contributions of (γ,X_0) and (γ,X_2) are not experimentally distinguishable. According to the simulation, ^{125}Te(γ,α_2) contributes 40% to the total α-particle yield at $11.0 < E_\gamma < 12.5$ MeV, in which the second excited state of the residual nucleus ^{121}Sn is an isomeric state with a long half-life of 43.9 years.

Figure 9 illustrates the proton spectra of (γ,p_0), (γ,p_3) and $(\gamma,p_{tot.})$ on ^{102}Pd (a) and ^{106}Cd (b) at $E_\gamma = 10.0$ MeV, and ^{115}Sn (c) and ^{117}Sn (d) at $E_\gamma = 12.5$ MeV. For these four targets, the sum of the yields of (γ,p_0) and (γ,p_3) can be measured, which prominently contributes the total proton yields. Still, the energy spectra show that the respective contributions of (γ,p_0) and (γ,p_3) cannot be recognized.

In Figure 10 the proton spectra of (γ,p_0), (γ,p_1), (γ,p_2) and $(\gamma,p_{tot.})$ on ^{74}Se at $E_\gamma = 10.0$
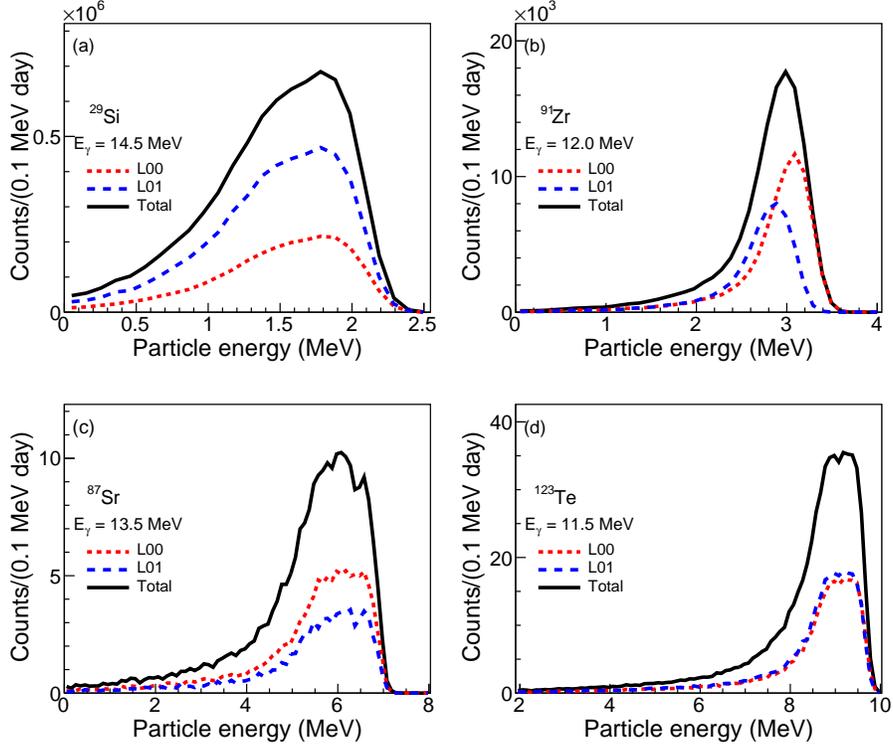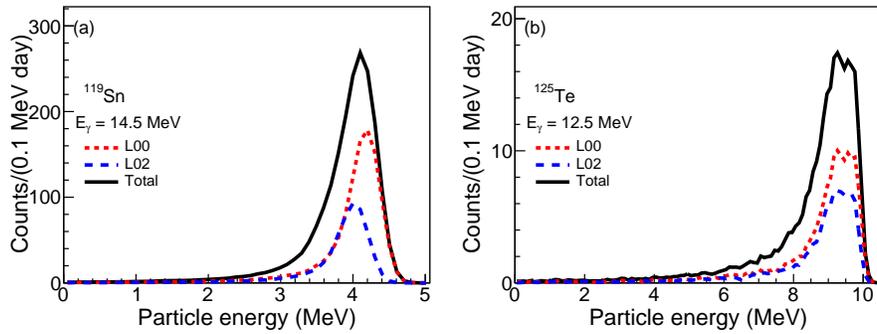
24

FIG. 7. Energy spectra of the protons emitted from (γ,p_0), (γ,p_1) and $(\gamma,p_{tot.})$ channels on ^{29}Si at $E_\gamma = 14.5$ MeV (a) and ^{91}Zr at $E_\gamma = 12.0$ MeV (b), and energy spectra of the α-particles emitted from (γ,α_0), (γ,α_1) and $(\gamma,\alpha_{tot.})$ channels on ^{87}Sr at $E_\gamma = 13.5$ MeV (c) and ^{123}Te at $E_\gamma = 11.5$ MeV (d). The results of $(\gamma,X_{tot.})$ $(X = p$ or $\alpha)$ include the contributions from all the (γ,X_i) channels with $0 \le i \le 10$.

FIG. 8. Energy spectra of the protons emitted from (γ,p_0), (γ,p_2) and $(\gamma,p_{tot.})$ channels on ^{119}Sn at $E_\gamma = 14.5$ MeV (a), and energy spectra of the α-particles emitted from (γ,α_0), (γ,α_2) and $(\gamma,\alpha_{tot.})$ channels on ^{125}Te at $E_\gamma = 12.5$ MeV (b). The results of $(\gamma,X_{tot.})$ $(X = p$ or $\alpha)$ include the contributions from all the (γ,X_i) channels with $0 \le i \le 10$.

MeV (a), and (γ,p_0), (γ,p_1), (γ,p_3) and $(\gamma,p_{tot.})$ on ^{84}Sr at $E_\gamma = 13.0$ MeV (b), as well as the α-particle spectra of (γ,α_0), (γ,α_1), (γ,α_4) and $(\gamma,\alpha_{tot.})$ on ^{50}V at $E_\gamma = 14.5$ MeV (c),
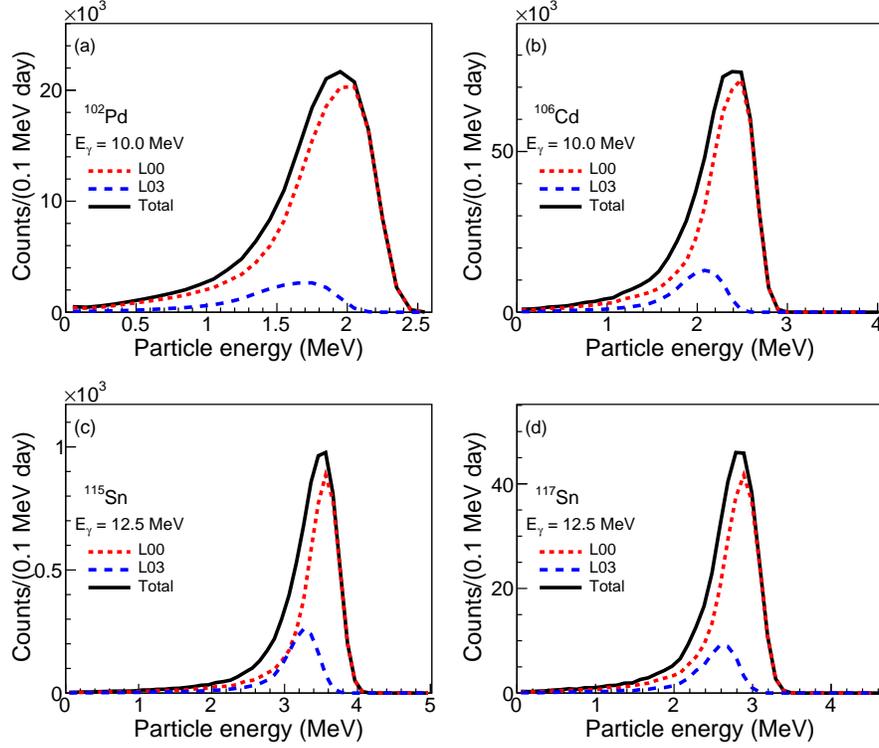
25

FIG. 9. Energy spectra of the protons emitted from (γ,p_0), (γ,p_3) and $(\gamma,p_{tot.})$ channels on ^{102}Pd (a) and ^{106}Cd (b) at $E_\gamma = 10.0$ MeV, and ^{115}Sn (c) and ^{117}Sn (d) at $E_\gamma = 12.5$ MeV. The results of $(\gamma,p_{tot.})$ include the contributions from all the (γ,X_i) channels with $0 \leq i \leq 10$.

and (γ,α_0), (γ,α_1), (γ,α_2) and $(\gamma,\alpha_{tot.})$ on $^{149}Sm+\gamma$ at $E_\gamma = 11.0$ MeV (d) are illustrated. For these four reactions, the total yields are contributed dominantly from three individual channels with the transitions to the ground and two excited states in the residual nucleus, so the measured yields are the sum of the yields of these three channels. However, each of the contributions from the three transitions cannot be respectively identified from the measurement.

Figure 11 demonstrates the proton spectra from $^{117}Sn+\gamma$ reaction and the α-particle spectra from $^{123}Te+\gamma$ reaction at $E_\gamma = 19.0$ MeV. The multiple emission channels (γ,np) and $(\gamma,n\alpha)$ are taken into account. It is found the energies of the emitted charged particles from the multiple channels are remarkably lower than the energies of the particles from (γ,X_i). Therefore, although the cross sections of multiple emissions are comparable to those of (γ,X_i), the multiple emission events can be readily removed by setting a proper threshold for the detection of the particle energies, and the interesting measurements of (γ,X_i) cannot be influenced.
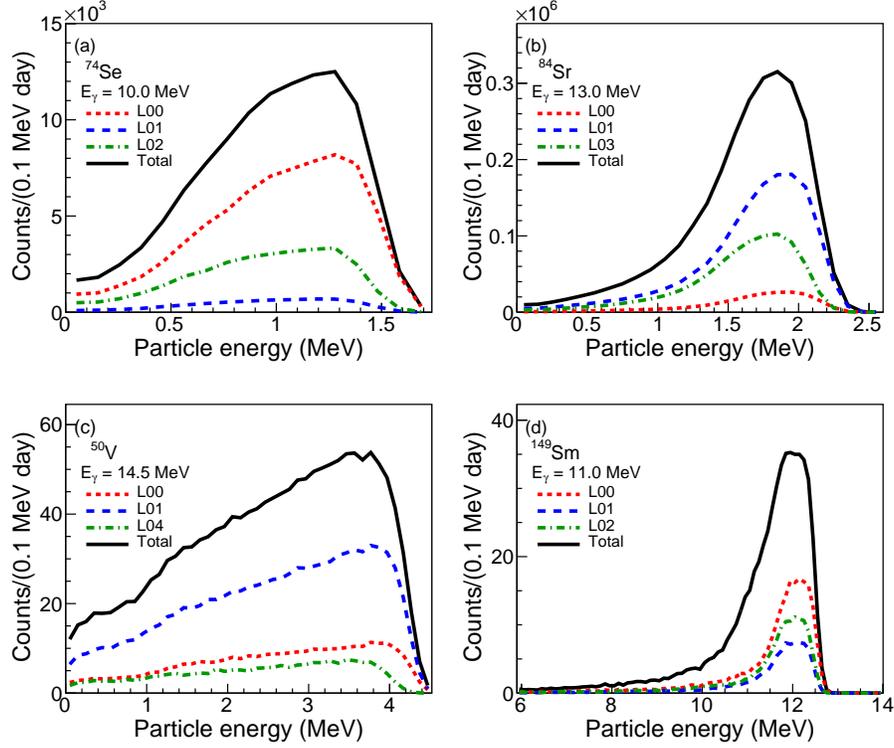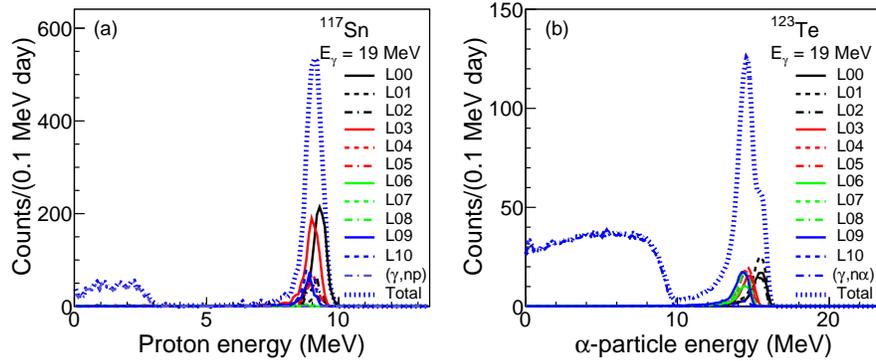
26

FIG. 10. Energy spectra of the protons emitted from (γ, p_0), (γ, p_1), (γ, p_2) and $(\gamma, p_{tot.})$ channels on ^{74}Se at $E_\gamma = 10.0$ MeV (a), and from (γ, p_0), (γ, p_1), (γ, p_3) and $(\gamma, p_{tot.})$ on ^{84}Sr at $E_\gamma = 13.0$ MeV (b). Energy spectra of the α-particles emitted from (γ, α_0), (γ, α_1), (γ, α_4) and $(\gamma, \alpha_{tot.})$ on ^{50}V at $E_\gamma = 14.5$ MeV (c), and (γ, α_0), (γ, α_1), (γ, α_2) and $(\gamma, \alpha_{tot.})$ on ^{149}Sm$+\gamma$ at $E_\gamma = 11.0$ MeV (d). The results of $(\gamma, X_{tot.})$ (X = p or α) include the contributions from all the (γ, X_i) channels with $0 \leq i \leq 10$.

FIG. 11. The energy spectra of the proton from $^{117}Sn+\gamma$ reaction and the α-particle from $^{123}Te+\gamma$ reaction at $E_\gamma = 19.0$ MeV. The results of (γ, X_i) channels are indexed by "L0i" for $0 \leq i \leq 10$, and the results of (γ, np) and $(\gamma, n\alpha)$ channels are indexed by "(γ, np)" and "$(\gamma, n\alpha)$", respectively. The label "Total" denotes the results counting all these considered contributions.

IV. SUMMARY

Capture and photodisintegration reactions proceeding on excited states of the target nucleus can significantly contribute to the astrophysical reaction rate. Those excited-state contributions are usually obtained from theoretical calculations but so far are inaccessible to a direct measurement. It is, however, possible to test and constrain theoretical models by measuring relevant nuclear properties in dedicated experiments, which can then provide better predictions of reaction rates. In this paper, we propose to measure the photon-induced reactions with proton and α-particle emissions, to investigate the nuclear transitions leading to specific excited states in the residual nucleus. The particle-transmission coefficients of the charged-particles for photodisintegration and capture reactions can be determined by the anticipated experimental result, which is important to improve the predictions of astrophysical reaction rates for astrophysical simulation of p nuclides production. For the (γ,p_i) reactions on seventeen targets and the (γ, α_i) reactions on seventeen targets, the sensitivity of the calculated cross sections to the nuclear properties is studied. It is found that the α-particle optical model potentials can considerably influence the relative contributions of (γ,α_i) cross sections to the total cross sections of $(\gamma,\alpha_{\mathrm{tot.}})$.

At the ELI-NP facility, a Variable Energy γ-ray (VEGA) system is being constructed, which opens new opportunities to experimentally study the photon-induced reactions of astrophysics interest. Based on the features of VEGA and the silicon strip array ELISSA developed at ELI-NP for charged-particle detection, GEANT4 simulations of the measurements of the photon-induced reactions with the proton emission on seventeen targets and the α-particle emission on seventeen targets are performed using the calculated cross sections. The yields of (γ,p_i) and (γ,α_i) channels are obtained from the simulation. The results reveal that, for the (γ,p) reaction on twelve targets (^{29}Si, ^{56}Fe, ^{74}Se, ^{84}Sr, ^{91}Zr, ^{96,98}Ru, ^{102}Pd, ^{106}Cd, and ^{115,117,119}Sn) and the (γ,α) reaction on five targets (^{50}V, ^{87}Sr, ^{123,125}Te, and ^{149}Sm), the yields of (γ,X_i) (X=p or α) channels with $i \neq 0$, namely the transitions to the exited states in the residual nucleus, are relevant and even dominant. Therefore, the feasibility of measuring these seventeen photo-induced reactions at VEGA+ELISSA is investigated further.

For each of the seventeen photon-induced reactions, in order to attain the minimum detectable limit of 100 counts per day for the total proton or α-particle yields, the minimum

required energies of the incident γ-beam (E_{low}) for the measurements are estimated. It is further found that for each considered reaction, the total yield of the charged-particle X may be dominantly contributed from one, two or three individual (γ,X_i) channels within a specific energy range of the incident γ-beam, i.e., [E_{low},E_{upper}]. If each of these photon-induced reactions are actually measured within their respective energy ranges, the sum of the yields of the dominant (γ,X_i) channels can be approximated by the measured yields of the charged particle X within acceptable uncertainty. This means that the yields of the (γ,X_i) channels prominently contributing to the total yields of X can be experimentally obtained. Therefore, it is important to determine the interval [E_{low},E_{upper}]. Using the simulated yields, such energy ranges [E_{low},E_{upper}] for each of the seventeen photon-induced reactions are derived.

Furthermore, for these seventeen targets, the energy spectra of (γ,X_i) channels are simulated with the incident γ-beam energies in their interval [E_{low},E_{upper}]. Based on the energy spectra, the identifications of the individual dominant (γ,X_i) channels are discussed. It is shown that the (γ,p_0) reaction channel for the targets of ^{56}Fe, ^{102}Pd and ^{106}Cd, and the (γ,p_1) channel for the targets of ^{96}Ru and ^{98}Ru can be exclusively determined. Therefore it becomes evident that a measurement of the photon-induced reactions with charged-particle emissions considered in this work is feasible with the VEGA+ELISSA system and will provide knowledge useful for nuclear astrophysics.

project AIM1848704-3.

REFERENCE

[1] E. M. Burbidge, G. R. Burbidge, W. A. Fowler, and F. Hoyle, Rev. Mod. Phys. **29**, 547 (1957).

[2] M. Arnould and C. Brihaye, Astronomy and Astrophysics **1**, 193 (1969).

[3] M. Arnould and S. Goriely, Physics Reports **384**, 1 (2003).

[4] M. Arnould, S. Goriely, and K. Takahashi, Physics Reports **450**, 97 (2007).

[5] F. Käppeler, R. Gallino, S. Bisterzo, and W. Aoki, Rev. Mod. Phys. **83**, 157 (2011).

[6] T. Rauscher, N. Dauphas, I. Dillmann, C. Fröhlich, Z. Fülöp, and G. Gyürky, Reports on Progress in Physics **76**, 066201 (2013).

[7] S. Woosley and W. Howard, The Astrophysical Journal Supplement Series **36**, 285 (1978).

[8] M. Rayet, M. Arnould, and N. Prantzos, Astronomy and Astrophysics **227**, 271 (1990).

[9] S. Fujimoto, M. Hashimoto, O. Koike, K. Arai, and R. Matsuba, The Astrophysical Journal **585**, 418 (2003).

[10] W. Rapp, J. Görres, M. Wiescher, H. Schatz, and F. Käppeler, The Astrophysical Journal **653**, 474 (2006).

[11] T. Hayakawa, N. Iwamoto, T. Kajino, T. Shizuma, H. Umeda, and K. Nomoto, The Astrophysical Journal **685**, 1089 (2008).

[12] C. Travaglio, R. Gallino, T. Rauscher, N. Dauphas, F. Röpke, and W. Hillebrandt, The Astrophysical Journal **795**, 141 (2014).

[13] M. Pignatari, K. Göbel, R. Reifarth, and C. Travaglio, International Journal of Modern Physics E **25**, 1630003 (2016).

[14] T. Rauscher, N. Nishimura, R. Hirschi, G. Cescutti, A. S. J. Murphy, and A. Heger, Monthly Notices of the Royal Astronomical Society **463**, 4153 (2016).

[15] N. Nishimura, G. Cescutti, R. Hirschi, T. Rauscher, J. d. Hartogh, and A. S. J. Murphy, arXiv preprint arXiv:1802.05836 (2018).

[16] N. Nishimura, T. Rauscher, R. Hirschi, A. S. J. Murphy, G. Cescutti, and C. Travaglio,

Monthly Notices of the Royal Astronomical Society **474**, 3133 (2017).

[17] W. A. Fowler, Q. J. Astron. Soc. **15**, 82 (1974).

[18] T. Rauscher, P. Mohr, I. Dillmann, and R. Plag, The Astrophysical Journal **738**, 143 (2011).

[19] T. Rauscher, The Astrophysical Journal Supplement Series **201**, 26 (2012).

[20] T. Rauscher, *Essentials of Nucleosynthesis and Theoretical Nuclear Astrophysics* (IOP Publishing, Bristol, 2020).

[21] T. Rauscher, International Journal of Modern Physics E **20**, 1071 (2011), arXiv:1010.4283 [nucl-th].

[22] T. Rauscher, The Astrophysical Journal Letters **755**, L10 (2012), arXiv:1207.1664 [astro-ph.SR].

[23] P. Norbert, I. Johann, and W. Volker, The European Physical Journal A - Hadrons and Nuclei **55**, 237 (2019).

[24] H. Utsunomiya, H. Akimune, S. Goko, M. Ohta, H. Ueda, T. Yamagata, K. Yamasaki, H. Ohgaki, H. Toyokawa, Y.-W. Lui, *et al.*, Physical Review C **67**, 015807 (2003).

[25] T. Shizuma, H. Utsunomiya, P. Mohr, T. Hayakawa, S. Goko, A. Makinaga, H. Akimune, T. Yamagata, M. Ohta, H. Ohgaki, *et al.*, Physical Review C **72**, 025808 (2005).

[26] H. Utsunomiya, S. Goriely, T. Kondo, T. Kaihori, A. Makinaga, S. Goko, H. Akimune, T. Yamagata, H. Toyokawa, T. Matsumoto, *et al.*, Physical Review Letters **100**, 162502 (2008).

[27] H. Utsunomiya, T. Renstrøm, G. Tveten, S. Goriely, T. Ari-Izumi, D. Filipescu, J. Kaur, Y.-W. Lui, W. Luo, S. Miyamoto, *et al.*, Physical Review C **99**, 024609 (2019).

[28] P. Mohr, K. Vogt, M. Babilon, J. Enders, T. Hartmann, C. Hutter, T. Rauscher, S. Volz, and A. Zilges, Physics Letters B **488**, 127 (2000).

[29] K. Vogt, P. Mohr, M. Babilon, J. Enders, T. Hartmann, C. Hutter, T. Rauscher, S. Volz, and A. Zilges, Physical Review C **63**, 055802 (2001).

[30] K. Sonnabend, K. Vogt, D. Galaviz, S. Müller, and A. Zilges, Physical Review C **70**, 035802 (2004).

[31] J. Hasper, S. Müller, D. Savran, L. Schnorrenberger, K. Sonnabend, and A. Zilges, Physical Review C **77**, 015803 (2008).

[32] J. Hasper, D. Galaviz, S. Müller, A. Sauerwein, D. Savran, L. Schnorrenberger, K. Sonnabend, and A. Zilges, Physical Review C **79**, 055807 (2009).

[33] C. Nair, A. Junghans, M. Erhard, D. Bemmerer, R. Beyer, P. Crespo, E. Grosse, M. Fauth,

K. Kosev, G. Rusev, *et al.*, Journal of Physics G: Nuclear and Particle Physics **35**, 014036 (2007).

[34] C. Nair, A. R. Junghans, M. Erhard, D. Bemmerer, R. Beyer, E. Grosse, K. Kosev, M. Marta, G. Rusev, K. D. Schilling, R. Schwengner, and A. Wagner, Physical Review C **81**, 055806 (2010).

[35] M. Erhard, A. Junghans, C. Nair, R. Schwengner, R. Beyer, J. Klug, K. Kosev, A. Wagner, and E. Grosse, Physical Review C **81**, 034319 (2010).

[36] O. Ershova, P. Adrich, H. Alvarez-Pol, F. Aksouh, T. Aumann, M. Babilon, K.-H. Behr, J. Benlliure, T. Berg, M. Boehmer, *et al.*, in *11th Symposium on Nuclei in the Cosmos*, Vol. 100 (SISSA Medialab, 2011) p. 232.

[37] O. Ershova, *Coulomb dissociation reactions on molybdenum isotopes for astrophysics applications*, Ph.D. thesis, Univ.-Bibliothek Frankfurt am Main (2012).

[38] T. Rauscher, in *11th International Conference on Nucleus-Nucleus Collisions (NN2012)*, Journal of Physics Conference Series, Vol. 420 (2013) p. 012138, arXiv:1209.4060 [astro-ph.HE].

[39] T. Rauscher, AIP Advances **4**, 041012 (2014), arXiv:1403.2015 [astro-ph.SR].

[40] T. Rauscher, Nuclear Physics News **3**, arXiv:1803.10581 (2018), arXiv:1803.10581 [astro-ph.HE].

[41] H. Lan, Y. Xu, W. Luo, D. Balabanski, S. Goriely, M. La Cognata, C. Matei, A. Anzalone, S. Chesnevskaya, G. Guardo, *et al.*, Physical Review C **98**, 054601 (2018).

[42] C. Ur, D. Balabanski, G. Cata-Danil, S. Gales, I. Morjan, O. Tesileanu, D. Ursescu, I. Ursu, and N. Zamfir, Nuclear Instruments and Methods in Physics Research Section B: Beam Interactions with Materials and Atoms **355**, 198 (2015).

[43] D. L. Balabanski, R. Popescu, D. Stutman, K. A. Tanaka, O. Tesileanu, C. A. Ur, D. Ursescu, and N. V. Zamfir, Europhysics Letters **117**, 28001 (2017).

[44] K. Homma, O. Tesileanu, L. D'alessi, T. Hasebe, A. Ilderton, T. Moritaka, Y. Nakamiya, K. Seto, H. Utsunomiya, and Y. Xu, Romanian Reports in Physics **68**, 233 (2016).

[45] O. Tesileanu, M. Gai, A. Anzalone, C. Balan, J. Bihalowicz, M. Cwiok, W. Dominik, S. Gales, D. Ghita, Z. Janas, D. Kendellen, M. L. Cognata, C. Matei, K. Mikszuta, C. Petcu, M. Pfutzner, T. Matulewicz, C. Mazzocchi, and C. Spitaleri, Romanian Reports in Physics **68**, 699 (2016).

[46] M. L. Cognata, A. Anzalone, D. Balabanski, S. Chesnevskaya, V. Crucillà, D. M. Filipescu,

G. Guardo, M. Gulino, D. Lattuada, C. Matei, R. Pizzone, S. Romano, C. Spitaleri, A. Taffara, O. Tesileanu, A. Tumino, and Y. Xu, Journal of Instrumentation **12**, C03079 (2017).

[47] W. Luo, Nuclear Science and Techniques **27**, 96 (2016).

[48] Z. C. Zhu, W. Luo, Z. C. Li, Y.-M. Song, X.-D. Wang, X.-L. Wang, and G.-T. Fan, Annals of Nuclear Energy **89**, 109 (2016).

[49] W. Luo, M. Bobeica, I. Gheorghe, D. M. Filipescu, D. Niculae, and D. L. Balabanski, Applied Physics B **122**, 8 (2016).

[50] M. Bobeica, D. Niculae, D. Balabanski, D. Filipescu, I. Gheorghe, D. Ghita, and W. Luo, Romanian Reports in Physics **68**, 847 (2016).

[51] W. Hauser and H. Feshbach, Physical Review **87**, 366 (1952).

[52] J. A. Holmes, S. E. Woosley, W. A. Fowler, and B. A. Zimmerman, Atomic Data and Nuclear Data Tables **18**, 305 (1976).

[53] J. J. Cowan, F.-K. Thielemann, and J. W. Truran, Physics Reports **208**, 267 (1991).

[54] S. Goriely, Nuclear Physics A **605**, 28 (1996).

[55] T. Rauscher, F.-K. Thielemann, and K.-L. Kratz, Physical Review C **56**, 1613 (1997).

[56] S. Goriely, S. Hilaire, and A. J. Koning, Astronomy and Astrophysics **487**, 767 (2008).

[57] Y. Xu, S. Goriely, A. J. Koning, and S. Hilaire, Physical Review C **90**, 024604 (2014).

[58] S. Hilaire, C. Lagrange, and A. Koning, Annals of Physics **306**, 209 (2003).

[59] P. Mohr, M. Babilon, D. Galaviz, K. Sonnabend, K. Vogt, and A. Zilges, Nuclear Physics A **719**, C90 (2003).

[60] H. Utsunomiya, P. Mohr, A. Zilges, and M. Rayet, Nuclear Physics A **777**, 459 (2006).

[61] P. Mohr, Zs. Fülöp, and H. Utsunomiya, Eur. Phys. J. A **32**, 357 (2007).

[62] T. Rauscher, Phys. Rev. C **81**, 045807 (2010), arXiv:1003.2802 [astro-ph.SR].

[63] W. Huang, G. Audi, M. Wang, F. G. Kondev, S. Naimi, and X. Xu, Chinese Physics C **41**, 030002 (2017).

[64] S. Goriely, N. Chamel, and J. M. Pearson, Physical Review C **88**, 061302 (2013).

[65] R. Capote, M. Herman, P. Obložinskỳ, P. Young, S. Goriely, T. Belgya, A. Ignatyuk, A. J. Koning, S. Hilaire, V. A. Plujko, *et al.*, Nuclear Data Sheets **110**, 3107 (2009).

[66] S. Goriely, S. Hilaire, and A. J. Koning, Physical Review C **78**, 064307 (2008).

[67] S. Goriely, E. Khan, and M. Samyn, Nuclear Physics A **739**, 331 (2004).

[68] S. Goriely and J.-P. Delaroche, Physics Letters B **653**, 178 (2007).

[69] P. Demetriou, C. Grama, and S. Goriely, Nuclear Physics A **707**, 253 (2002).

[70] A. Gilbert and A. G. W. Cameron, Canadian Journal of Physics **43**, 1446 (1965).

[71] W. Dilg, W. Schantl, H. Vonach, and M. Uhl, Nuclear Physics A **217**, 269 (1973).

[72] A. V. Ignatyuk, J. L. Weil, S. Raman, and S. Kahane, Physical Review C **47**, 1504 (1993).

[73] S. Goriely, F. Tondeur, and J. Pearson, Atomic Data and Nuclear Data Tables **77**, 311 (2001).

[74] S. Hilaire, M. Girod, S. Goriely, and A. J. Koning, Physical Review C **86**, 064317 (2012).

[75] A. Koning and J. Delaroche, Nuclear Physics A **713**, 231 (2003).

[76] J. P. Jeukenne, A. Lejeune, and C. Mahaux, Physics Reports **25**, 83 (1976).

[77] J.-P. Jeukenne, A. Lejeune, and C. Mahaux, Physical Review C **16**, 80 (1977).

[78] E. Bauge, J. Delaroche, and M. Girod, Physical Review C **58**, 1118 (1998).

[79] S. Goriely, S. Hilaire, M. Girod, and S. Péru, Physical Review Letters **102**, 242501 (2009).

[80] J. Kopecky and M. Uhl, Physical Review C **41**, 1941 (1990).

[81] D. Brink, Nuclear Physics **4**, 215 (1957).

[82] P. Axel, Physical Review **126**, 671 (1962).

[83] S. Goriely and E. Khan, Nuclear Physics A **706**, 217 (2002).

[84] S. Goriely, Physics Letters B **436**, 10 (1998).

[85] I. Daoutidis and S. Goriely, Physical Review C **86**, 034328 (2012).

[86] S. Goriely, S. Hilaire, S. Péru, and K. Sieja, Physical Review C **98**, 014327 (2018).

[87] S. Watanabe, Nuclear Physics **8**, 484 (1958).

[88] L. McFadden and G. Satchler, Nuclear Physics **84**, 177 (1966).

[89] V. Avrigeanu, P. Hodgson, and M. Avrigeanu, Physical Review C **49**, 2136 (1994).

[90] M. Nolte, H. Machner, and J. Bojowald, Physical Review C **36**, 1312 (1987).

[91] V. Avrigeanu, M. Avrigeanu, and C. Mănăilescu, Physical Review C **90**, 044612 (2014).

[92] D. Lattuada, D. Balabanski, S. Chesnevskaya, M. Costa, V. Crucillà, G. Guardo, M. La Cognata, C. Matei, R. Pizzone, S. Romano, *et al.*, *EPJ Web of Conferences*, **165**, 01034 (2017).

[93] "Micron semiconductor," `https://www.micron.com`.

[94] S. Chesnevskaya, D. Balabanski, D. Choudhury, P. Constantin, D. Filipescu, D. Ghita, G. Guardo, D. Lattuada, C. Matei, A. Rotaru, and A. State, Journal of Instrumentation **13**, T05006 (2018).

[95] G. L. Guardo, A. Anzalone, D. Balabanski, S. Chesnevskaya, W. Crucillá, D. Filipescu, M. Gulino, M. La Cognata, D. Lattuada, C. Matei, *et al.*, *EPJ Web of Conferences*, **165**,

01026 (2017).

[96] W. Luo, W. Xu, Q. Pan, Z. An, X. Cai, G. Fan, G. Fan, Y. Li, B. Xu, Z. Yan, *et al.*, Nuclear Instruments and Methods in Physics Research Section A: Accelerators, Spectrometers, Detectors and Associated Equipment **660**, 108 (2011).

[97] W. Luo, H.-Y. Lan, Y. Xu, and D. L. Balabanski, Nuclear Instruments and Methods in Physics Research Section A: Accelerators, Spectrometers, Detectors and Associated Equipment **849**, 49 (2017).

[98] J. Duenas, D. Mengoni, V. Parkar, R. Berjillos, M. Assie, D. Beaumel, A. Sánchez-Benítez, and I. Martel, Nuclear Instruments and Methods in Physics Research Section A: Accelerators, Spectrometers, Detectors and Associated Equipment **676**, 70 (2012).

[99] M. Munch, C. Matei, S. D. Pain, M. T. Febbraro, K. A. Chipps, H. J. Karwowski, C. A. Diget, A. Pappalardo, S. Chesnevskaya, G. L. Guardo, D. Walter, D. L. Balabanski, F. D. Becchetti, C. R. Brune, K. Y. Chae, J. Frost-Schenk, M. J. Kim, M. S. Kwag, M. La Cognata, D. Lattuada, R. G. Pizzone, G. G. Rapisarda, G. V. Turturica, C. A. Ur, and Y. Xu, Physical Review C **101**, 055801 (2020).